Volume 1 | Number 1 | Jan 2013 | Pages 1–100

Journal of
Materials Chemistry A

Materials for energy and sustainability
www.rsc.org/materialsA

Li⁺

ROYAL SOCIETY OF CHEMISTRY

ROYAL SOCIETY OF CHEMISTRY

www.rsc.org/materialsA

Journal of Materials Chemistry A

ARTICLE

Engineering Superlyophobic Surfaces on Curable Materials Based on Facile and Inexpensive Microfabrication

Lifang Yuan, ‡[a] Tianzhun Wu,*‡[b] Weiji Zhang, [a] Shiquan Ling, [b] Rong Xiang, [a] Xuchun Gui, [a] Yuan Zhu [a] and Zikang Tang*[ac]

[a] School of Physics and Engineering, Sun Yat-Sen University, Guangzhou 510275, China.
[b] Shenzhen Institutes of Advanced Technology, Chinese Academy of Sciences, Shenzhen 518055, China. E-mail: tz.wu@siat.ac.cn
[c] State Key Laboratory of Optoelectronic Materials and Technologies, Sun Yat-Sen University, Guangzhou 510275, China. Email: tangzk@mail.sysu.edu.cn
‡ These Authors contributed equally to this work.

This paper proposes a facile, versatile, and low-cost approach for batch production of engineering superlyophobic surfaces (SLS, simultaneously superhydrophobic and superoleophobic) on various curable materials. Based on the soft replication using poly(dimethylsiloxane) (PDMS) as the intermediate mold, T-shape overhang microstructures on Si and dual-resist masters have been transferred to curable materials including poly(methyl methacrylate) (PMMA), PDMS and glass resin. As-fabricated polymer SLS replicas exhibit high structure fidelity, comparable nonwettability and excellent reproducibility for both water and oil during the 10×10 replication, and possess new features such as tunable transparency. The proposed microfabrication approach for SLS decouples the material and process dependence, greatly dilutes the fabrication cost and enables high-performance SLS on a wide range of materials, which may initialize the broad applications of engineering SLS for various low-contamination, low-adhesion and self-cleaning liquid handling in academy, industry and daily life.

Journal of Materials Chemistry A   RSC**Publishing**

ARTICLE

Introduction

Superhydrophobic surfaces, which show high contact angle (CA) typically above 150° and low contact angle hysteresis (CAH) for water and other aqueous solutions, have been studied for several decades, developed by various techniques,[1-10] and widely used for water-handling applications such as anti-ice or anti-frost coatings,[11-14] stain-resistant textiles,[15, 16] and various anti-fouling, self-cleaning surfaces.[17-22] Nevertheless, they usually do not repel low-surface-tension liquids (typical surface tension 15-35 mN m^{-1}) such as oil, organic solutions and aqueous solutions with surfactants or high temperature.[23] This can be briefly explained in Fig.1a. For superhydrophobic surfaces typically with trapezoid or pillar microstructures, oil pressure P_{oil} generated by the Laplace pressure and gravity drives the contact line (CL) to move downward. Due to the low intrinsic CA (Young's CA, θ_Y), surface tension γ_{lv} acting on the CL yields downward pressure P_{CL} which accelerates the collapse of the composite Cassie-Baxter (C-B) meta-stable state.[24] Here subscripts l, v stand for liquid and vapor, respectively. To generate upward γ_{lv} or P_{CL} to balance P_{oil}, well-designed overhang (or re-entrant) structures are found crucial to obtain oleophobicity.[25-27] Oil can be pinned on the bottom part of beads (Fig. 1c) or sharp corners (Fig. 1b, d). According to the Gibbs inequation,[26, 28] the maximum pinning CA θ_{pin} on the corner with solid angle δ (defined as the angle on the CL formed by the slope tangent and the liquid-air interface, as shown in Fig.1) is enlarged to $\theta_{pin}=180°-\delta+\theta_Y$, thus a small δ ensures a high θ_{pin}, resulting in the upward γ_{lv} and P_{CL} to balance P_{oil}. Hence on the carefully designed and controlled overhang microstructures, both water and oil can be effectively suspended by surface tension. As the extension and enhancement of superhydrophobic surfaces, superlyophobic surfaces (SLS) with such overhang features,[26, 29-31] also called omniphobic surfaces[32-35] or superamphiphobic

Journal of Materials Chemistry A   RSC**Publishing**

ARTICLE

surfaces,[36–39] are simultaneously superhydrophobic and superoleophobic, which exhibit excellent nonwetting performances for almost any liquid, no matter Newton and non-Newton,[40] high-surface-tension or low-surface-tension.[32] Due to their universal repellence and huge potential for academic and industrial applications, recently intensive research interests have been focused on the fabrication of SLS based on either random structures (nanoparticles,[39, 41, 42] nanopores,[43, 44] nanowires,[31] etc.) or regular patterns (microhoodoos,[25] T-shape micropillars,[26, 29, 30] inverse trapezoids,[45] textile fibers,[40, 46] etc.). There are also some reports on characterization and modeling of interesting liquid behaviors on SLS,[26, 30, 32, 47, 48] as well as some application demonstrations for microfluidics[30] and chemical shielding.[40] However, existing fabrication technologies for SLS so far suffer from two major difficulties, which stem from the great fabrication challenge of special overhang micro/nano structures. Firstly, various micro/nano fabrication techniques of SLS highly rely on specific and few materials such as Si,[25, 26, 29, 30] poly(dimethylsiloxane) (PDMS),[33, 45] and some nanomaterials,[39, 42, 49, 50] only on which overhang structures can be created. As the results, new fabrication or synthesis techniques have to be developed for particular materials. Such coupling of materials and processes is a great restriction for SLS fabrication, performances and applications. Secondly, low-cost and robust SLS remains a significant challenge. Their geometrics such as pitches (P), pillar diameters (D), overhang profiles and so on, need to be well controlled, since the nonwetting performances including CA, CAH and pressure stability are highly related to these geometric details.[26, 30, 32, 49] For random structures, it would be essentially difficult to control geometric details and structure uniformity on a large area, although they may be created in a cost-effective manner through chemical synthesis,[50] electrospinning[46] or even candle soot deposition.[39] On the other hand, regular structures can be precisely defined in the

Journal of Materials Chemistry A   RSC**Publishing**

fashion called "what you see is what you get (WYSIWYG)" by using fabrication technologies of micro electromechanical systems (MEMS), and their processes can be compatible with IC batch production. However, MEMS fabrication for SLS typically requires expensive and demanding processes such as XeF_2 etching,[25, 26] reactive ion etching (RIE), deep reactive ion etching (DRIE)[29, 30] and 3D diffuser lithography.[45]

To unblock the two bottlenecks, herein we propose a facile and inexpensive microfabrication approach for high-performance and mass-production of SLS on various curable materials. By employing PDMS as the intermediate mold, T-shape micropillars on Si master or inverse T-shape microcavities on dual-layer resist can be precisely and readily transferred to various polymer substrates. Such replication solves the first bottleneck by decoupling materials and fabrication processes for SLS, hence feasible to a wide range of inexpensive, curable materials with mild phase-change conditions, such as paper pulp, powder, resin, plastics and various polymer with useful properties. Multiple transfer of T-shape pillars using inexpensive PDMS soft mold helps to break the second bottleneck. PDMS has excellent flexibility, high replication precision (up to nm order[51]) and high durability (at least 100 times without degradation[52, 53]), which make it very popular as the intermediate mold.[54, 55] T-shape pillar is chosen because we have demonstrated its mechanical robustness, easy profile control and excellent suspending ability for both water and oil,[26] and they can be easily demolded with small undercuts. Furthermore, by selectively developing dual-layer resist[56] to form inverse T-shape microcavities and casting PDMS, T-shape micropillars with controllable undercuts are obtained, which is much more facile and inexpensive than typical dry etching.[25, 26, 29, 30] Based on these methods, batch replication of low-cost, high-performance SLS becomes possible on various curable materials with new features (flexibility, transparency,

Journal of Materials Chemistry A   RSCPublishing

ARTICLE

etc.). Considering the significantly increased material choices, reduced fabrication complexity and cost, as well as excellent replication performances, we believe this strategy enables the mass production of engineering SLS for broad academic, industrial or daily-life applications.

Microfabrication strategy

To enable well-defined T-shape microstructures on various materials, the proposed microfabrication strategy using PDMS-based soft replication and dual-resist photolithography is illustrated in Fig. 2 (see details in the Experimental Section). We firstly demonstrated the soft replication method using the Si master (Fig. 2g-j), which was fabricated using DRIE process with thermally grown SiO_2 over the Si substrate (Fig. 2a and b) as described in our previous reports.[26, 30] Then they were treated with fluorinated self-assembled monolayer (F-SAM) to facilitate easy demolding. After that, PDMS was dispensed and cured as the intermediate mold to further transfer patterns to many daughter SLS on curable materials, as long as they were in the liquid phase or dissolved in solution before curing, and their curing temperatures were not too high (less than 343 °C, the decomposition temperature of PDMS). Then they may be coated with low-surface-tension fluorocarbon using C_4F_8 plasma[26] or F-SAM to achieve the superlyophobicity. Note that small undercuts of T-shape pillars will not be damaged thanks to the flexible and stretchable elastomer, which is superior for the overhang structure transfer. The repeatable and durable use of Si master and PDMS molds enables high-throughput and large-scale SLS replication. Benefited from the dual-replication process, the number of replicas is calculated as "number of PDMS molds (M) × number of daughter replicas (N)". Since Si master is much more durable than PDMS (M>N≥100), one Si master can produce more than 10,000 replicas. Note that PDMS and many curable

Journal of Materials Chemistry A

ARTICLE

materials are inexpensive, this method is believed to greatly dilute the replica cost and promote the low-cost application of SLS.

To further reduce the fabrication complexity and cost, we replaced the Si master with a polymer one where inverse T-shape microcavities were fabricated in a single photo-lithography process based on dual-layer resist (Fig. 2c-f). After spin-coating two resist layers on the Si substrate, thin electron-beam resist AR-P 5460 (not sensitive to UV) and thick photoresist SU-8, SU-8 was patterned and AR-P resist was over-developed in several minutes to yield a controlled undercut. After casting and demolding PDMS against the hard-baked dual-resist layers, the T-shape intermediate PDMS mold was achieved, which can be further modified with better hydrophobicity using F-SAM or C_xF_y deposition.

Experimental

Fabrication of Si master

SiO_2 (300 nm-thick) was thermally grown on the Si (100) wafer, and a thin positive resist AZ1500 (1.5 μm-thick, AZ Electronic Materials) was spin-coated and patterned using the standard photolithography. Exposed SiO_2 was etched by RIE using CF_4 plasma, followed by dicing and photoresist stripping. The T-shaped profile was etched using DRIE (MUC 21, SPTS Co.) by tuning the SF_6 etching rate and the C_4F_8 deposition rates. After O_2 plasma cleaning, samples were treated by vapor-phase F-SAM using 1H,1H,2H,2H-perfluorooctyltrichlorosilane (PFTS, n-$CF_3(CF_2)_5(CH_2)_2SiCl_3$) at 140 °C for 4 min (see more details in previous reports[26, 30]).

Fabrication of polymer master

A layer of AR-P 5460 resist (1.5 μm-thick, Allresist Gmbh) was spin-coated on the clean Si wafer and baked at 160 °C for 5 min. Then, SU8-2050 (20 μm-thick, Microchem Co.) was

Journal of Materials Chemistry A   RSCPublishing

spin-coated and patterned using the standard photolithography. After the SU-8 development, the wafer was immersed in ethanol to avoid bubbles, and then developed using the AR developer 300-47 (1:3 diluted by DI water to extend the development time). Then cast PDMS (Sylgard 184, Dow Corning Co.) with base:curing agent=10:1 against the dual-resist sample using the standard soft lithography. After peeling the PDMS master with T-shape micropillars was obtained. C_4F_8 plasma was used to deposit fluorocarbon coating (80 nm-thick) on the PDMS master for easy demolding.

Soft replication

PDMS was poured into a clean dish with a Si or PDMS master with a fluorocarbon coating, degassed and baked (70 °C for 45 min). After peeling the PDMS mold from the master, thermally curable materials like PDMS, poly(methyl methacrylate) (PMMA, 410k Dalton, Wako Co.) and glass resin (GR 650, Techneglas Co.) were poured onto the PDMS intermediate mold, degassed, and cured at 70 °C for 2 h (for PDMS and PMMA) and 90 °C for 3 h (glass resin), respectively. PDMS was peeled off from these curable materials and the polymer replicas were achieved.

Sample characterization

Before taking pictures using scanning electron microscope (SEM) (S4800, Hitachi Co.) a gold layer (~20 nm-thick) was sputtered onto polymer samples for better conductivity. Static and dynamic CAs were measured using the contact angle meter (DSA 30, Kruss Gmbh) at room temperature, and each CA value was measured for at least 5 times by fitting tangents near the CL. Water and hexadecane droplets were less than 5 μL so that gravity can be ignored. The optical transmission of PDMS and PMMA samples (thickness ~2 mm) was measured by an UV-visible spectrophotometer (Shimadzu Co.).

Journal of Materials Chemistry A　　　RSC**Publishing**

Results and discussion

Microstructures

A typical microscopic picture of as-fabricated T-shape micropillars on Si with 300 nm-thick SiO$_2$ cap and undercut ~100 nm is shown in Fig. 3a using SEM. The etching depth was ~30 μm, the undercut was ~100 nm, the pitch P=50 μm and diameters D=15, 25, 35 μm, yielding solid fraction f_s (defined as the solid/liquid area fraction in a unit structure) from 0.07 to 0.38. According to our previous study,[26, 30] these geometric parameters enables high CA, low CAH and good pressure stability for both water and oil. As the demonstration of soft replication, two commonly used materials, glass resin and PMMA were cast against the PDMS mold (Fig. 3b) as shown in Fig. 3c and d, which exhibited high fidelity of their Si master.

The microstructures of polymer replicas with different undercuts and materials (PDMS and PMMA) fabricated using the dual-resist photolithography are shown in Fig. 4a-c. The cap thickness was ~1.5 μm and the pillar height was ~20 μm. As plot in Fig. 4d, the undercut is approximately linear with the AR-P resist developing time. By developing from 1 min to 2.5 min, undercuts varied from 1 μm to 8 μm.

Nonwetting performances

Two probing liquids, de-ionized (DI) water (surface tension γ_{lv}=72 mN m^{-1}) and hexadecane (γ_{lv}=27 mN m^{-1}) were used to characterize the nonwetting performances on each master and replica. Fig. 5a-c show comparable static CA θ_s>150° for both liquids on a Si master (solid fraction f_s=0.07) and its PMMA and glass resin replica. Similar results were found for the PDMS master (Fig. 5d) and its PMMA replica (Fig. 5e) based on the dual-resist photo-lithography and soft replication. Clearly these static CAs were fairly close due to the excellent replication precision.

Journal of Materials Chemistry A   RSCPublishing

ARTICLE

To quantitatively compare the nonwetting performances between masters and replicas, experimental data of θ_s, advancing CAs θ_{adv} and receding CA θ_{rec} are plot in Fig. 6. For Si and its first PMMA replica these CAs for both water and hexadecane were close, while for PDMS master and its PMMA replica, although water and hexadecane θ_s and θ_{adv} were also comparable for different f_s, hexadecane θ_{rec} on the PDMS sample was significantly larger than that on PMMA, especially for high f_s=0.385. This deviation may be caused by the soft, porous nature of swelling PDMS which incurred more dissipation for moving contact lines. We compared the measured θ_s with the theoretical equilibrium CA θ_{CB} using the C-B model, written as $\cos\theta_{CB} = r_f\, f_s\cos\theta_Y + f_s$ -1= $f_s(\cos\theta_s +1)$ -1, where r_f is the roughness of wetted surface, defined as the actual wetted surface area divided by its projected surface area. The measured data of static and dynamic CAs for water and hexadecane on flat Si, PMMA and PDMS after F-SAM are listed in ESI†. Note that although both θ_{CB} and θ_s decreased with increasing f_s, hexadecane θ_s was significantly higher than its theoretical prediction θ_{CB} for high f_s, consistent with previous reports.[25, 26, 30, 47] This deviation indicates that the C-B model is not accurate for low-surface-tension liquid on SLS, which involves complicated contact line profiles due to the overhang structures, and calls for new wetting models to understand more solid-liquid details of SLS.

Reproducibility

Reproducibility of daughter replicas is crucial for mass production of engineering SLS. Fig. 7 showed the evolution of θ_s of daughter SLS during the 10×10 replication from three Si masters and three PDMS intermediate molds based on the dual-layer resist with varying f_s. For Si-based PMMA daughters after the F-SAM treatment, the average value and scattering range of θ_s was (161±3.6)° for water, (145.8±3.5)° for hexadecane when f_s=0.07, and

Journal of Materials Chemistry A   RSC**Publishing**

ARTICLE

(151.7±5.6)° for water, (141.1±3.6)° for hexadecane when f_s=0.385. On the other hand, for resist-based PDMS daughters, these values were respectively (140.7±2.7)° for water, (134.1±2.4)° for hexadecane when f_s=0.11, and (141.1±2.4)° for water, (131.2±6.7)° for hexadecane when f_s=0.385. Generally the daughter θ_s were close to their master values, and the scattering ranges sometimes increased slightly with increasing f_s. It seems that these daughters did not show inferior CA performances with increasing replication times, and the scattering range was acceptable, which can be further improved by microfabrication optimization. However, the C-B model gave poor estimation for most of measured θ_s. As shown with solid and dashed lines in Figure 7, water θ_{CB} was roughly in an agreement with scattering θ_s for Si-based PMMA replicas, yet it was higher than those for resist-based PDMS replicas, supposed to be affected by some rough and hydrophilic defects on the resist-based replicas (see Fig. 4). Again, most scattering hexadecane θ_s data for f_s>0.19 were significantly higher than their θ_{CB}, indicating the C-B model fails to capture the contact line physics of low-surface-tension oil on SLS.

We also compared the dynamic CAs on Si-based PMMA daughter SLS with their theoretical values in Fig. 8 using the model proposed by Choi et al.,[42] who suggested that for SLS with discrete pillars, θ_{adv}=180° and $\theta_{rec}=\sqrt{f_s}\,(\cos\theta_s+1)$-1. According to the calculation, most of measured water θ_{rec} and all measured hexadecane θ_{rec} were respectively smaller and larger than this model predicted. To our best knowledge there is rare literature on modeling static and dynamic CAs on SLS with varying f_s and materials, and more research efforts should focus on the oil behavior on SLS.

Optical transparency

Journal of Materials Chemistry A   RSC**Publishing**

ARTICLE

Extended choices of curable materials endow SLS with very useful new features, such as chemical inertness, scalability, flexibility and transparency. As an example, Fig. 9 shows the optical transmission of PMMA replica (based on the Si master) and PDMS replica (based on the resist master). The transmittance of smooth PMMA was above 70% in the visible light wavelength range, while its SLS samples with f_s=0.19 and 0.38 had slightly reduced transparency down to respectively its 82% and 77% at the wavelength 600 nm. The PDMS film had a higher transmission around 90%, and the transmission of its SLS was still around 75% when f_s=0.38. One can expect that reducing f_s helps to increase the transparency. Their transparency and superlyophobicity were shown in Fig. 9, where various droplets including DI water, hexadecane and ethanol (γ_{lv}=22.3 mN m^{-1}) can stand as balls on these transparent polymer SLS, and our laboratory logo can be clearly read through them.

Conclusions

To unblock the two bottlenecks of SLS fabrication, namely the coupling of materials and processes and the demanding fabrication requirement for constructing controllable overhang micro/nano structures, we have proposed a novel fabrication approach to transfer 3D T-shape microstructures to various curable materials using PDMS as the intermediate mold. 10×10 daughter replicas from both Si master etched by DRIE and dual-resist master formed in a single photo-lithography process have been demonstrated on widely used polymers (PMMA, PDMS, glass resin) with high structure fidelity, comparable static and dynamic CAs and excellent reproducibility, as well as tunable transparency. Existing CA models (by Cassie-Baxter and Choi et al.) could not provide accurate prediction for most measured CAs on these materials. The deviations were more pronounced for oil, and call for further theoretical exploration on modeling liquid behaviors on various SLS.

Journal of Materials Chemistry A

ARTICLE

References

1   H. Y. Erbil, A. L. Demirel, Y. Avci, and O. Mert, *Science*, 2003, **299**, 1377–1380.

2   A. Lafuma and D. Quere, *Nat Mater*, 2003, **2**, 457–460.

3   K. K. S. Lau, J. Bico, K. B. K. Teo, M. Chhowalla, G. A. J. Amaratunga, W. I. Milne, G. H. McKinley, and K. K. Gleason, *Nano Lett.*, 2003, **3**, 1701–1705.

4   M. Nosonovsky and B. Bhushan, *Curr. Opin. Colloid Interf. Sci.*, 2009, **14**, 270–280.

5   Z. Guo, W. Liu, and B.-L. Su, *J. Colloid Interf. Sci.*, 2011, **353**, 335–355.

6   Y. Xiu, D. W. Hess, and C. P. Wong, *J. Colloid Interf. Sci.*, 2008, **326**, 465–470.

7   Y. Y. Yan, N. Gao, and W. Barthlott, *Adv. Colloid Interf. Sci.*, 2011, **169**, 80–105.

8   E. Ueda and P. A. Levkin, *Adv. Mater.*, 2013, **25**, 1234–1247.

9   X. Yin, D. Wang, B. Yu, and F. Zhou, *RSC Adv.*, 2014, **4**, 3611–3614.

10   Y. Wang, W. Wang, L. Zhong, J. Wang, Q. Jiang, and X. Guo, *Appl. Surf. Sci.*, 2010, **256**, 3837–3840.

11   P. Kim, T.-S. Wong, J. Alvarenga, M. J. Kreder, W. E. Adorno-Martinez, and J. Aizenberg, *ACS Nano*, 2012, **6**, 6569–6577.

12   S. A. Kulinich and M. Farzaneh, *Appl. Surf. Sci.*, 2009, **255**, 8153–8157.

Journal of Materials Chemistry A   RSC**Publishing**

13   K. K. Varanasi, T. Deng, J. D. Smith, M. Hsu, and N. Bhate, *Appl. Phys. Lett.*, 2010, **97**, 234102.

14   S. A. Kulinich and M. Farzaneh, *Langmuir*, 2009, **25**, 8854–8856.

15   M. Shateri Khalil-Abad and M. E. Yazdanshenas, *J. Colloid Interf. Sci.*, 2010, **351**, 293–298.

16   J. Zimmermann, F. A. Reifler, G. Fortunato, L.-C. Gerhardt, and S. Seeger, *Adv. Func. Mater.*, 2008, **18**, 3662–3669.

17   T. Sun, L. Feng, X. Gao, and L. Jiang, *Acc. Chem. Res.*, 2005, **38**, 644–652.

18   O.-U. Nimittrakoolchai and S. Supothina, *J. Eur. Ceram. Soc.*, 2008, **28**, 947–952.

19   B. Bhushan, Y. C. Jung, and K. Koch, *Langmuir*, 2009, **25**, 3240–3248.

20   S. Kim, E. Cheung, and M. Sitti, *Langmuir*, 2009, **25**, 7196–7199.

21   J. Zhu, C.-M. Hsu, Z. Yu, S. Fan, and Y. Cui, *Nano Lett.*, 2010, **10**, 1979–1984.

22   J. Zhang, G. Pu, and S. J. Severtson, *ACS Appl Mater Interf.*, 2010, **2**, 2880–2883.

23   Y. Liu, X. Chen, and J. H. Xin, *J. Mater. Chem.*, 2009, **19**, 5602.

24   A. Cassie and S. Baxter, *Trans. Faraday Soc.*, 1944, **40**, 546–551.

25   A. Tuteja, W. Choi, M. Ma, J. M. Mabry, S. A. Mazzella, G. C. Rutledge, G. H. McKinley, and R. E. Cohen, *Science*, 2007, **318**, 1618–1622.

26   T. Wu and Y. Suzuki, *Sens. Actuat. B Chem.*, 2011, **156**, 401–409.

27   A. Marmur, *Langmuir*, 2008, **24**, 7573–7579.

28   J. W. Gibbs, *The scientific papers of J. Willard Gibbs (reprint)*, Dover, New York, 1961, vol. 1.

29   A. Ahuja, J. A. Taylor, V. Lifton, A. A. Sidorenko, T. R. Salamon, E. J. Lobaton, P. Kolodner, and T. N. Krupenkin, *Langmuir*, 2008, **24**, 9–14.

Journal of Materials Chemistry A   RSC**Publishing**

30   T. Wu and Y. Suzuki, *Lab. Chip*, 2011, **11**, 3121–3129.

31   V. A. Lifton and S. Simon, *J. Microelectromechan. Syst.*, 2011, **20**, 73–82.

32   A. Tuteja, W. Choi, J. M. Mabry, G. H. McKinley, and R. E. Cohen, *Proc. Natl. Acad. Sci.*, 2008, **105**, 18200–18205.

33   R. Dufour, M. Harnois, Y. Coffinier, V. Thomy, R. Boukherroub, and V. Senez, *Langmuir*, 2010, **26**, 17242–17247.

34   S. M. Kang, S. M. Kim, H. N. Kim, M. K. Kwak, D. H. Tahk, and K. Y. Suh, *Soft Matter*, 2012, **8**, 8563.

35   S. P. R. Kobaku, A. K. Kota, D. H. Lee, J. M. Mabry, and A. Tuteja, *Angew. Chem. Int. Ed.*, 2012, **51**, 10109–10113.

36   H. J. Li, X. B. Wang, Y. L. Song, Y. Q. Liu, Q. S. Li, L. Jiang, and D. B. Zhu, *Angew. Chem.-Int. Ed.*, 2001, **40**, 1743–1746.

37   G. Choi, J. Park, J. Ha, W. Kim, and H. Lim, *Macromol. Mater. Eng.*, 2010, **295**, 995–1002.

38   H.-J. Butt, C. Semprebon, P. Papadopoulos, D. Vollmer, M. Brinkmann, and M. Ciccotti, *Soft Matter*, 2012, **9**, 418–428.

39   X. Deng, L. Mammen, H.-J. Butt, and D. Vollmer, *Science*, 2012, **335**, 67 –70.

40   S. Pan, A. K. Kota, J. M. Mabry, and A. Tuteja, *J. Am. Chem. Soc.*, 2013, **135**, 578–581.

41   B. Leng, Z. Shao, G. de With, and W. Ming, *Langmuir*, 2009, **25**, 2456–2460.

42   A. Steele, I. Bayer, and E. Loth, *Nano Lett.*, 2009, **9**, 501–505.

43   L. Cao, T. P. Price, M. Weiss, and D. Gao, *Langmuir*, 2008, **24**, 1640–1643.

44   X. Wang, X. Liu, F. Zhou, and W. Liu, *Chem. Commun.*, 2011, **47**, 2324–2326.

Journal of Materials Chemistry A   RSC**Publishing**

ARTICLE

45   M. Im, H. Im, J.-H. Lee, J.-B. Yoon, and Y.-K. Choi, *Soft Matter*, 2010, **6**, 1401–1404.

46   W. Choi, A. Tuteja, S. Chhatre, J. M. Mabry, R. E. Cohen, and G. H. McKinley, *Adv. Mater.*, 2009, **21**, 2190–2195.

47   W. Choi, A. Tuteja, J. M. Mabry, R. E. Cohen, and G. H. McKinley, *J. Colloid Interf. Sci.*, 2009, **339**, 208–216.

48   M. Im, H. Im, J.-H. Lee, J.-B. Yoon, and Y.-K. Choi, *Langmuir*, 2010, **26**, 17389–17397.

49   A. K. Kota, W. Choi, and A. Tuteja, *MRS Bull.*, 2013, **38**, 383–390.

50   J. Zhang and S. Seeger, *Angew. Chem. Int. Ed.*, 2011, **50**, 6652–6656.

51   B. D. Gates, Q. Xu, M. Stewart, D. Ryan, C. G. Willson, and G. M. Whitesides, *Chem. Rev.*, 2005, **105**, 1171–1196.

52   A. Kumar, H. A. Biebuyck, and G. M. Whitesides, *Langmuir*, 1994, **10**, 1498–1511.

53   R. S. Kane, S. Takayama, E. Ostuni, D. E. Ingber, and G. M. Whitesides, *Biomater.*, 1999, **20**, 2363–2376.

54   G. Shao, J. Wu, Z. Cai, and W. Wang, *Sens. Actuat. Phys.*, 2012, **178**, 230–236.

55   G. Zhuang and J. P. Kutter, *J. Micromech. Microeng.*, 2011, **21**, 105020.

56   D. Sameoto and C. Menon, *J. Micromech. Microeng.*, 2009, **19**, 115002.

Journal of Materials Chemistry A

RSC**Publishing**

ARTICLE
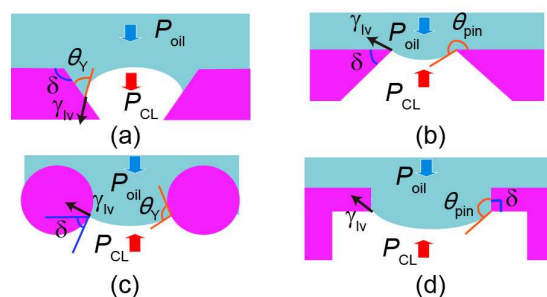
Fig.1 Illustration showing that overhang microstructure is crucial for obtaining oleophobicity. (a) A typical trapezoidal microstructure with solid angle $\delta \geq 90°$ where γ_{lv} yields downward P_{CL}, and the C-B state collapses. (b) An inverse-trapezoidal microstructure with $\delta < 90°$ where γ_{lv} yields upward P_{CL} to balance P_{oil}. (c) A ball-like microstructure can pin oil on the bottom part so that upward P_{CL} may balance P_{oil}. (d) A T-shape microstructure with $\delta = 90°$ also enables upward P_{CL}.

Journal of Materials Chemistry A   RSC**Publishing**

ARTICLE
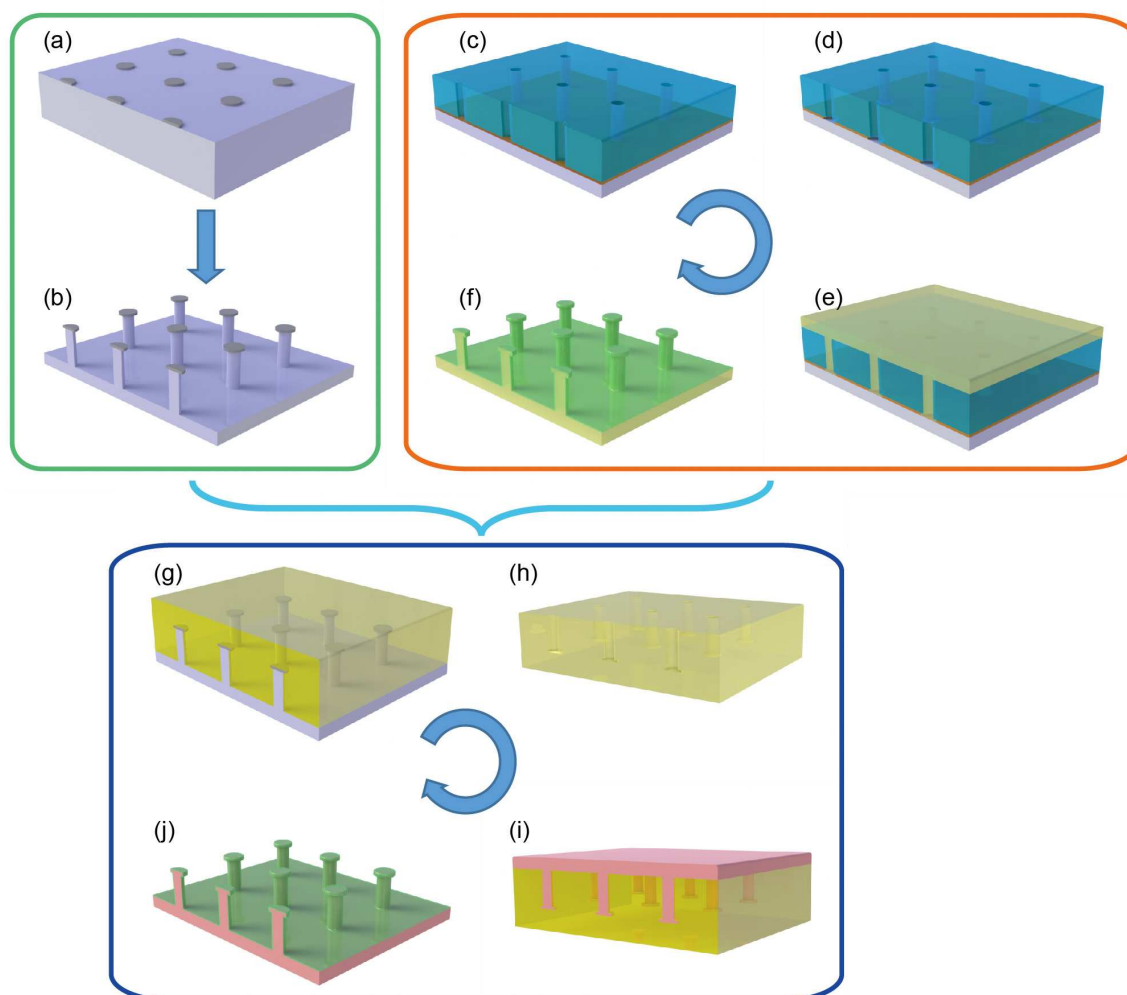
Fig. 2 Schematic illustration of the microfabrication strategy. (a) Patterning SiO_2 cap on Si. (b) Microfabrication of T-shaped pillars using DRIE. (c) Spin-coating ARP-5460 thin resist and SU-8 thick resist, and patterning SU-8. (d) Over-developing ARP-5460 resist to form inverse T-shape microcavities. (e) Casting PDMS using the standard soft lithography. (f) Conformally coating C_xF_y on PDMS T-shape pillars using C_4F_8 plasma. (g) Casting PDMS onto Si (or PDMS) master. (h) Peeling PDMS intermediate mold off the master. (i) Pouring curable

Journal of Materials Chemistry A RSC**Publishing**

materials onto the PDMS mold and curing with proper thermal or UV conditions. (j) Low-surface-tension treatment with F-SAM or C_xF_y coating.
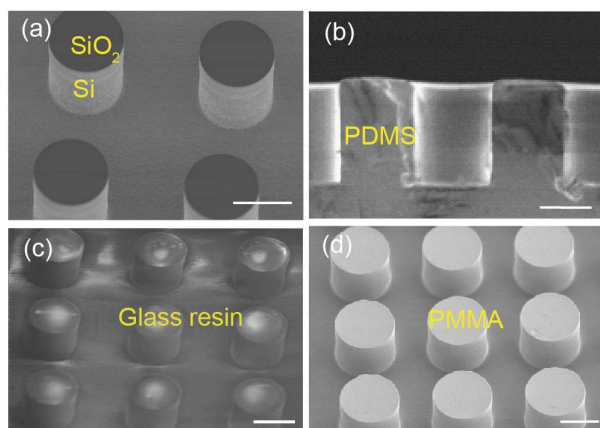
Fig. 3 SEM pictures of Si master and its replicas based on DRIE and soft replication. (a) Bird's view of SiO_2 caps on the Si substrate with small undercut ~100 nm. (b) Cross-sectional view of the PDMS intermediate mold. (c) Glass resin replica (d) PMMA replica. Scale bar 20 μm for all.

Journal of Materials Chemistry A

ARTICLE
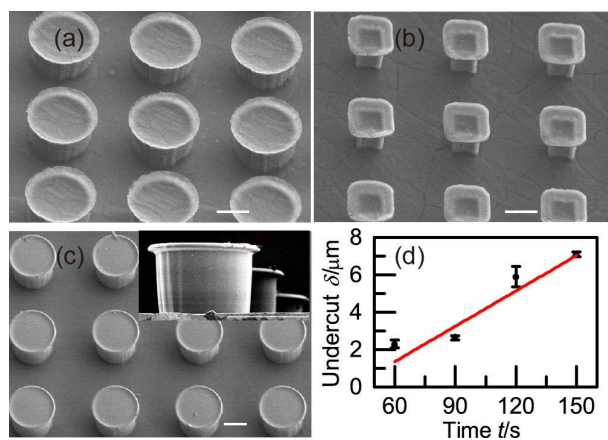
Fig. 4 SEM pictures of PMMA (a, b) and PDMS (c) replicas based on the dual-resist photo-lithography and soft replication. Insert is the cross-sectional view of PDMS replica. (d) Undercut length varied with the developing time of AR-P resist. Scare bar 20 μm for all.

Journal of Materials Chemistry A   RSC**Publishing**

ARTICLE
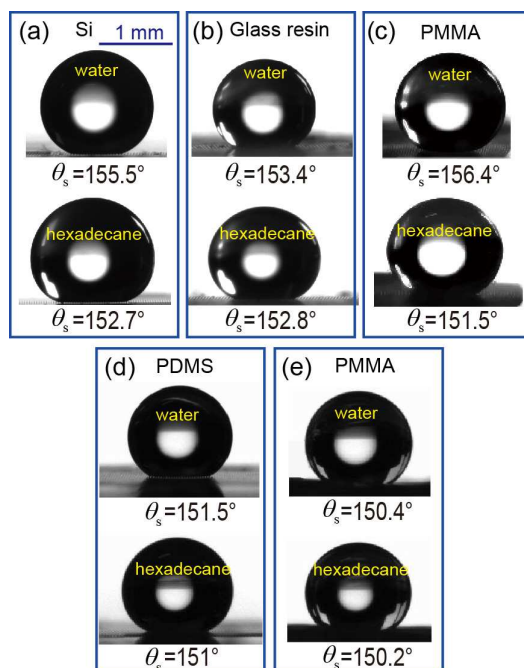
Fig. 5 Static CAs for water (72 mN m^{-1}) and hexadecane (27 mN m^{-1}) on the SLS with same f_s =0.07 (*P*=50 μm, *D*=15 μm) and different substrates. (a)-(c) Si master and its PMMA and glass resin replicas. (d)-(e) PDMS mold and its PMMA replica using the resist master. Scale bar 1 mm for all.

Journal of Materials Chemistry A   RSC**Publishing**

ARTICLE
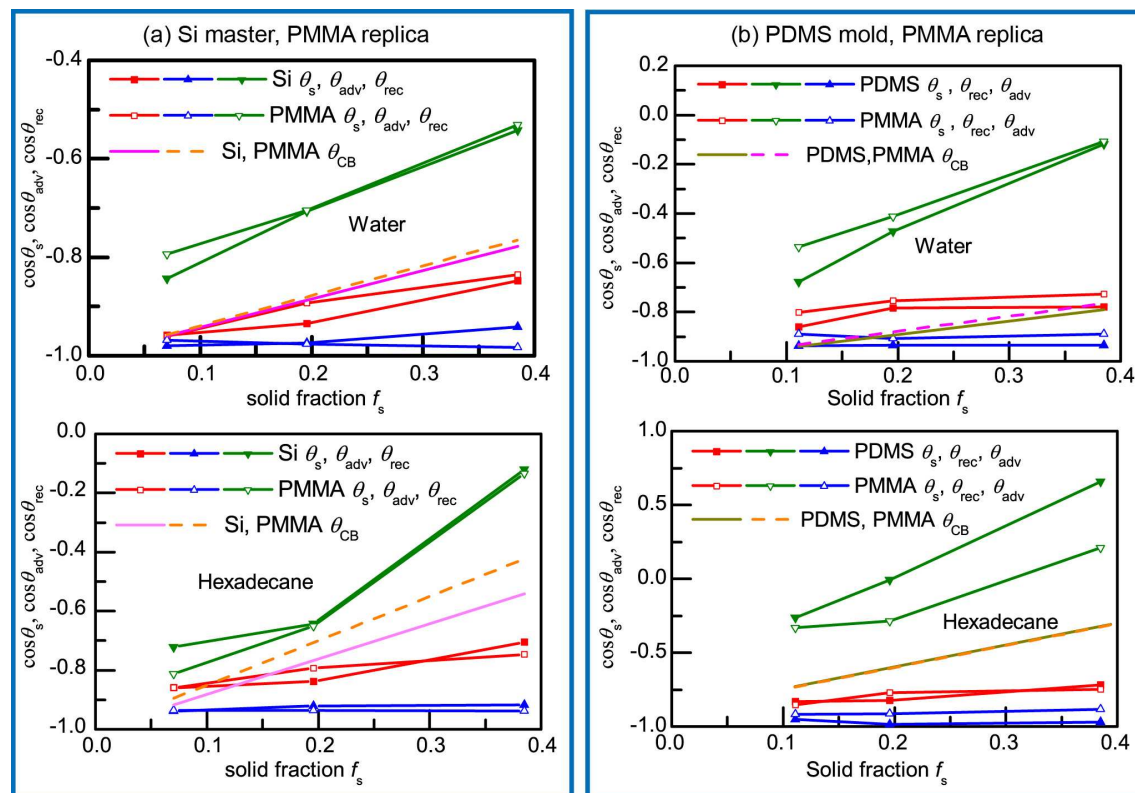
Fig. 6 Comparison of static and dynamic CAs on polymer replicas and their corresponding masters. All CAs for water and hexadecane were comparable for master SLS and their PMMA replicas except the hexadecane θ_{rec} on PMMA replicas based on the PDMS mold using the dual-resist method. θ_{CB} had significant deviations with measured θ_s especially for hexadecane at high f_s.

Journal of Materials Chemistry A   RSC**Publishing**
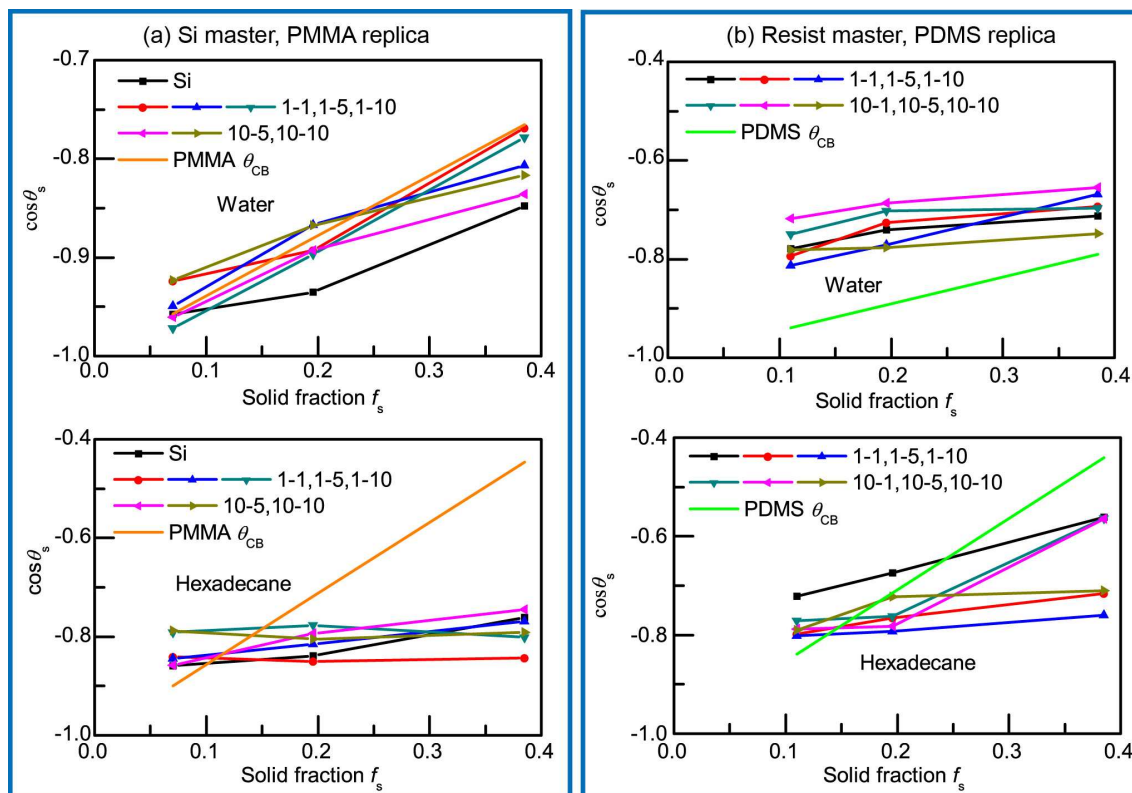
Fig. 7 Comparison of static CAs during 10×10 soft replication. (a) Plot for Si-based PMMA replicas; (b) Plot for resist-based PDMS replicas. For the legend "a-b", "a" represents the replication times of the PDMS intermediate mold, and "b" represents the replication times of the polymer daughter replica. θ_s did not show systematic degrade during the replication, and the scattering range did not clearly depend on f_s. However, the C-B model could not provide accurate prediction for most measured θ_s.

Journal of Materials Chemistry A   RSC**Publishing**
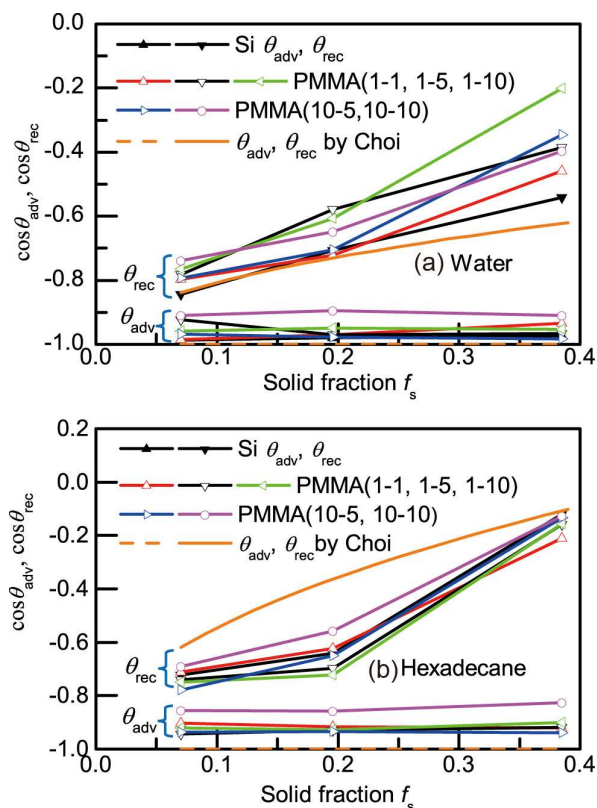
ARTICLE

Fig. 8 Evolution of dynamic CAs of PMMA replicas and their Si master. (a) Dynamic CAs for water. (b) Dynamic CAs for hexadecane. Dashed and solid curves represent respectively theoretical θ_{adv} and θ_{rec} predicted by Choi et al.

Journal of Materials Chemistry A

ARTICLE
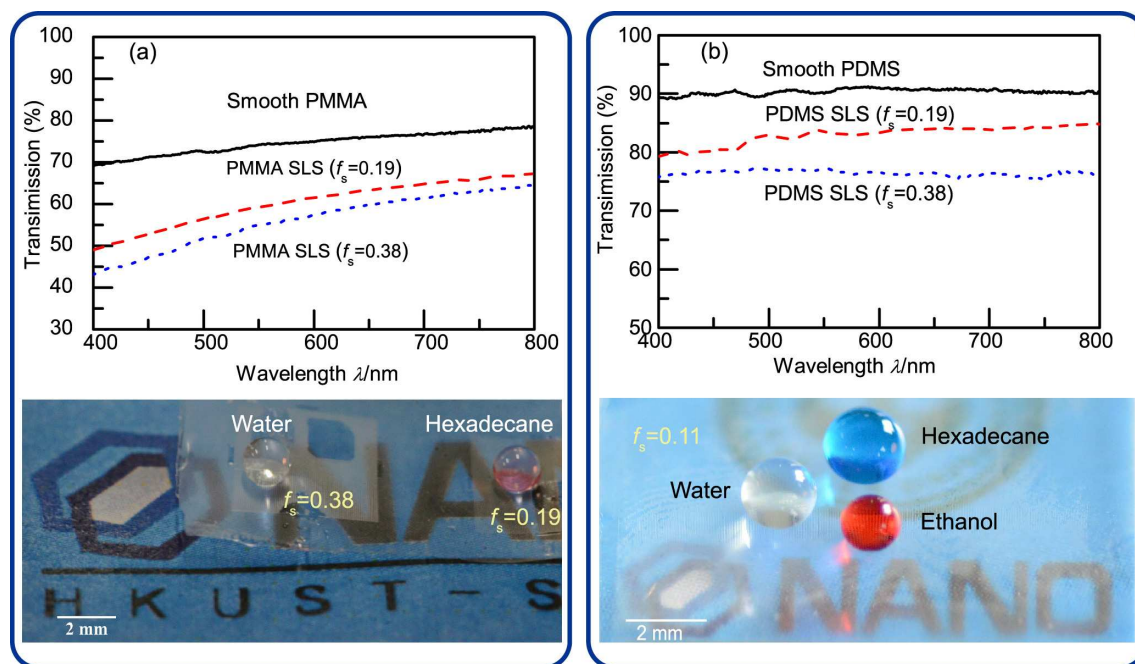
Fig. 9 Optical transmission measurement of PMMA (a) and PDMS (b) SLS and their corresponding smooth samples (thickness ~2 mm). Water and oil droplets sit on these transparent SLS on a paper printed with the logo.